CIMAC CONGRESS 25
ZURICH, MAY 19 – 23, 2025

2025 | 384

Effects of water blending on spray characteristics and combustion performance of methanol

Dual Fuel / Gas / Diesel

Tianlong Lu, Tianjin University

Dongming Zhang, Tianjin University
Zhen Zeng, Tianjin University
Minghao Xiahou, Tianjin University
Haoye Liu, Tianjin University
Tianyou Wang, Tianjin University

This paper has been presented and published at the 31st CIMAC World Congress 2025 in Zürich, Switzerland. The CIMAC Congress is held every three years, each time in a different member country. The Congress program centres around the presentation of Technical Papers on engine research and development, application engineering on the original equipment side and engine operation and maintenance on the end-user side. The themes of the 2025 event included Digitalization & Connectivity for different applications, System Integration & Hybridization, Electrification & Fuel Cells Development, Emission Reduction Technologies, Conventional and New Fuels, Dual Fuel Engines, Lubricants, Product Development of Gas and Diesel Engines, Components & Tribology, Turbochargers, Controls & Automation, Engine Thermondynamis, Simulation Technologies as well as Basic Research & Advanced Engineering. The copyright of this paper is with CIMAC. For further information please visit https://www.cimac.com.

ABSTRACT

For a diesel-ignited high-pressure direct injection methanol engine with high methanol substitution ratios, water blending is an effective approach to reduce NOx emissions. The blending of water into methanol alters the physical properties, thereby potentially changing the spray characteristics under high injection pressure conditions. In this study, the effects of water blending on spray characteristics, combustion, and emission performance were investigated experimentally on a constant volume chamber and refitted dual-fuel diesel engine test bench. The vapor-phase and liquid-phase spray morphology of methanol were captured by backlight illumination and Schlieren imaging technology; the results indicate that changes in fuel physical properties have a minor impact on vapor-phase spray characteristics but significantly affect the liquid-phase spray characteristics. The liquid-phase spray of methanol is different compared with that of diesel, exhibiting shorter spray penetration length, and smaller projection area. Water blending into methanol leads to a significant increase in the liquid-phase spray penetration distance and spray area. With the engine experiment, the results indicate that CA10 and CA50 delayed with the increased water content, and the intensity of the post-combustion (CA50-CA90) was enhanced. As the water content increases, the gross work and exhaust losses decrease, exhaust losses gradually decrease, and heat transfer losses and incomplete combustion losses increase slightly. A water content of 10%, 20%, and 30% were required to meet Tier III emissions standards for low, medium, and high load conditions, respectively.

1 INTRODUCTION

Global climate and environmental changes pose serious challenges to human economic and social development. The transition to a low-carbon or even zero-carbon economy has become an inevitable trend in global economic development. The global goal of "carbon neutrality" by 2050 will accelerate the transformation of traditional industries, and low-carbon technologies will become a new driving force for global economic growth [1]. In the field of automotive engines, countries around the world, including China, have formulated increasingly stringent plans and regulations to reduce CO_2 emissions [2]. The large-scale shipping industry is responsible for more than 80% of the world's international trade, with CO_2 emissions accounting for 2% to 3% of the world's total emissions, making it a key sector in the global low-carbon economy. The International Maritime Organization (IMO) has been actively promoting the reduction of greenhouse gas emissions in the shipping industry [3]. In 2011, the IMO introduced the Energy Efficiency Design Index (EEDI), which requires a 30% reduction in CO_2 emissions by 2025 compared to 2013 when the EEDI entered its third phase. In 2023, the IMO further proposed that CO_2 emissions per voyage in international shipping should be reduced by at least 40% by 2030 compared to 2008, to achieve net-zero emissions by around 2050 [4].

From the perspective of achieving low-carbon emissions in ships, replacing traditional fossil fuels such as diesel and heavy oil with widely available and renewable carbon-neutral fuels can completely resolve the carbon emission problem. Methanol, as a liquid carbon-neutral fuel at normal temperature and pressure, is characterized by safety, ease of storage, and a mature fuel distribution system [5]. Using methanol as a fuel for marine engines is an important solution for achieving low-carbon emissions in the short and medium term [6]. In 2018, the IMO explicitly listed methanol/ethanol fuel ship technologies as a high-priority project and approved the Interim Guidelines for the Safety of Ships Using Methyl/Ethyl Alcohol as Fuel, addressing bottlenecks in methanol transportation and usage [7]. The global carbon neutrality goal for 2050 and the zero-emission trend in the shipping industry have created a broad application market for methanol-fueled engines. At the same time, from 2025 to 2050, methanol will also be highly competitive in price compared to traditional fossil fuels. Methanol is low-cost to produce and can reduce operating expenses when used as fuel [8]. Methanol can be derived from biomass and waste [9-11], and with technological advancements, renewable methanol produced from hydrogen and carbon dioxide from renewable energy sources can further expand the use of methanol as a chemical feedstock [12]. The use of methanol to replace diesel as fuel in compression-ignition engines can improve combustion and emission performance in the short term while offering significant carbon reduction potential in the medium to long term.

Methanol has a low cetane number (3-5), good volatility, and high latent heat of vaporization, whereas diesel has a high cetane number (40-55), poor volatility, and low latent heat of vaporization [13]. Therefore, the combustion structure and pattern of methanol are significantly different from traditional diesel combustion, involving more diverse and complex combustion technologies [14]. The application research of methanol engines has gone through three stages: methanol premixed ignition combustion, diesel-ignited low-pressure intake methanol compression, and diesel-ignited high-pressure direct injection methanol combustion [14-20]. The diesel-methanol high-pressure dual-injection combustion technology, which ignites diesel at the top dead center to trigger combustion of the non-premixed fuel mixture formed by high-pressure direct-injected methanol, can effectively solve issues such as low methanol substitution rates and abnormal combustion phenomena encountered in intake methanol injection combustion [21-22]. However, research on this technology is still limited. The marine methanol engines launched by MAN and Wärtsilä have all adopted this diesel-methanol high-pressure dual-injection combustion technology [23-24], but detailed combustion and emission data have not been publicly released. Relevant research from abroad is scarce. Chalmers University of Technology [21] pioneered research on diesel-methanol high-pressure dual-injection combustion technology, while Aalto University in Finland [22] conducted preliminary studies on the combustion process of this technology using a modified diesel engine. In their research, they employed a structure with a centrally positioned high-pressure methanol injector and an additional diesel injector on one side. They also adjusted the spray holes of the side-mounted diesel nozzle to ensure it only injected igniting diesel toward the piston center, avoiding the spraying of excessive fuel on the wet wall. The combustion process of the diesel-methanol high-pressure dual-injection combustion mode includes three stages: diesel ignition combustion, diesel diffusion combustion with early methanol ignition, and methanol diffusion combustion. The load range covers from 4.2 bar to 13.8 bar IMEP (corresponding to about 2 bar to 12 bar BMEP). Since methanol undergoes combustion and heat release similar to direct injection diffusion combustion after diesel ignition, the heat release rate is controllable, with a high substitution rate of

up to 95% at high loads, and the maximum indicated thermal efficiency can reach 45% [21-22].

The high-pressure pathway features injecting methanol directly into the combustion chamber near the top dead center at a high injection pressure (typically higher than 60 MPa), which significantly enhances the controllability of the methanol mixture and combustion process, providing the possibility of achieving the methanol substitution rate >95% [25]. The high-pressure combustion technology for methanol has called on higher demands on understanding and quantifying the spray characteristics of high-pressure direct injection of methanol, which is of great significance in the relative engine design and simulation model development. However, the research focusing on the high-pressure spray characteristics of methanol is scarce. Ghosh et al. [26] investigated the influence of background density, background temperature, and injection pressure on the spray characteristics of methanol at the injection pressure range from 20 MPa to 48 MPa. The results indicated that under evaporative conditions an increase in background density significantly reduced the vapor-phase and liquid-phase spray penetration of methanol. Increasing the injection pressure enhanced the vapor-phase spray penetration, with little impact on the liquid penetration. Wang et al. [27] conducted a comparative study on the spray characteristics of methanol and diesel at the high-pressure range from 60 MPa to 140 MPa. The results revealed that under the same background and high-pressure injection conditions, methanol exhibited lower vapor penetration and a larger vapor-phase spray cone angle. At a background temperature of 800 K, with an injection pressure of 100 MPa, the quasi-steady state liquid penetration of methanol was 4.6% lower than that of diesel, and the quasi-steady state liquid spray projection area decreased by 52%.

The characteristic of high oxygen content and the absence of carbon-carbon bonds in methanol molecules result in a significantly lower tendency for soot formation during combustion compared to conventional hydrocarbon fuels [5]. However, NOx emissions from methanol combustion are generally in the same order of magnitude as those from traditional hydrocarbon fuels [28]. Svensson et al. [28] compared the soot formation during the combustion of methanol and diesel under internal combustion engine time scales. It found that the soot formation peninsula in the phi-T diagram for methanol is much smaller than that for diesel, but the NOx formation peninsula is essentially similar to diesel. Therefore, under high-pressure direct injection compression ignition conditions, the combustion process of methanol results in almost negligible soot emissions, but NOx emissions remain significant [14][22][28]. Due to the high heat capacity and cooling effects of water evaporation, the NOx formation in combustion could be largely suppressed by mixing a certain percentage of water in methanol. MAN ES [29] first announced water in methanol as a method to obtain Tier III compliance on a marine engine and started the investigation of this combustion principle in 2019. Recently, Kunkel et al. [30] demonstrated the impact of water content on the emission characteristics of a MAN engine of diesel-pilot high-pressure direct injection compression ignition of methanol. The results showed that an increased water content significantly lowered NOx emission. The NOx emissions already met Tier III standards without the need for additional after-treatment devices when the water content reached around 30%.

In summary, for diesel-methanol high-pressure dual-injection combustion, the addition of water to methanol is an effective method to reduce nitrogen oxide emissions and lower engine manufacturing and operational costs. However, the blending of water significantly alters the physical properties of methanol, which in turn affects the spray characteristics. In this study, firstly the physical properties of methanol with different water contents were measured and presented. Then, the high-pressure direct injection spray characteristics of methanol were tested under thermodynamic conditions close to the compression ignition (CI) engines, and the impact of water blending on methanol spray characteristics was examined and analyzed considering the inherent reasons for physical property alterations by water blending. Subsequently, the combustion and emission performance under various loads were explored based on the thermodynamic single-cylinder dual direct injection engine platform. This study can guide the design of methanol high-pressure direct-injection CI engines as well as the efficient and clean combustion technology of methanol under high-pressure injection conditions.

2 FUEL PROPERTIES OF METHANOL AND METHANOL-WATER BLENDS

The methanol used in this study was anhydrous methanol of analytical grade purity with a concentration of 99.5%, and diesel is standard #0 diesel. Deionized water is used to prepare methanol-water blends. The density, viscosity, and surface tension of fuels affect the break-up process, the boiling point, specific heat capacity, and latent heat of vaporization affect the evaporation process, which in turn affects the high-pressure spray characteristics. Therefore, before carrying out the methanol spray visualization experiments, the above physical properties of the

test fuel were first determined. The physical properties of anhydrous methanol (MeOH), #0 diesel, and methanol-water blends with 10% wt, 20% wt, and 30% wt water (W10, W20, and W30) are shown in Table 1.

Table 1. Physical properties of test fuels.

Physical property	MeOH	Diesel	W10	W20	W30
Density (g/cm^3)	0.79	0.86	0.804	0.822	0.841
Viscosity (mPa·s)	0.6	3.7	0.677	0.821	0.987
Surface tension (N/m)	0.023	0.029	0.049	0.041	0.035
Boiling point at 1 bar (K)	338	450-640	338-373	338-373	338-373
Heat capacity (kJ/(kg·k))	2.53	1.9	2.715	2.88	3.045
Latent heating value (kJ/kg)	1109	270	1224.1	1339.2	1454.3

Within the water content range of 10-30% wt, the density, viscosity, and surface tension of methanol-water blends all increase with the increasing water content, while the effect of water blending on the boiling point is relatively small. In this range, the density, viscosity, surface tension, and boiling point of methanol-water blends are all lower than those of diesel. It is worth noting that as the water content increases, the specific heat capacity and latent heat of vaporization significantly increase (with a 31% increase in specific heat capacity at 30% wt water content), which are considerably higher than that of diesel.

3 EXPERIMENTAL SETUP AND METHODOLOGY

3.1 High-pressure Spray Testing System and Imaging Methods

3.1.1 Spray Visualization Testing System

The high-pressure direct injection spray characteristics of methanol and other test fuels were studied using a constant-volume chamber visualization experimental system which is depicted in Figure 1. This system consists of a constant-volume chamber system, a high-pressure fuel injection system, an intake and exhaust system, an optical system, and a computer control system. Quartz glass is installed on both sides of the constant-volume chamber to provide a visual passage for spray visualization. The background temperature and pressure inside the constant-volume chamber are adjusted by controlling the power of the heating wire and the valve opening of the high-pressure nitrogen. The injector used in this study is a single-hole diesel injector with a nozzle diameter of 0.2 mm. A fuel pump driven by compressed air with a compression ratio of 202:1 is used to increase the injection pressure of methanol, with a maximum pressure reaching 120 MPa. The injection operation is controlled by an internal control system, which can adjust parameters such as injection timing and injection duration simultaneously.

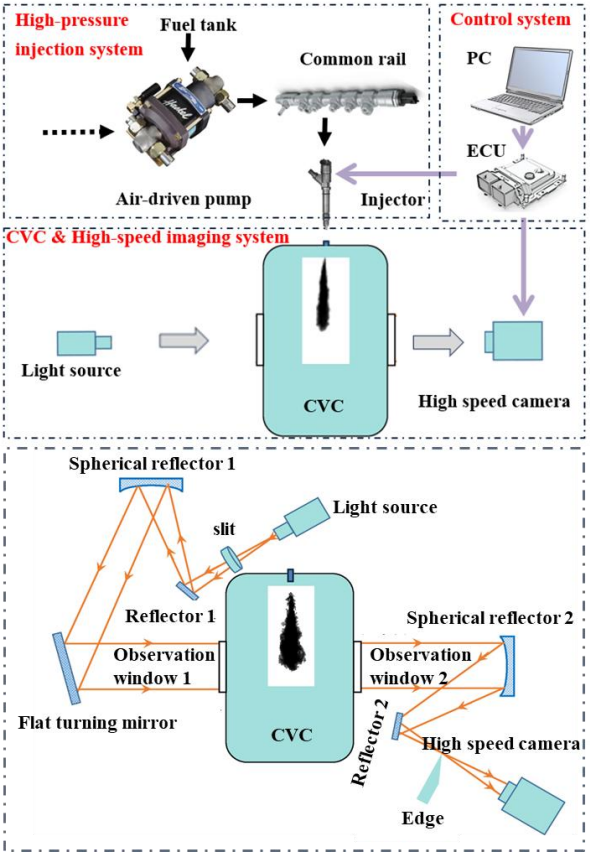

Figure 1. Constant-volume chamber visualization experimental system.

3.1.2 Spray Image Processing Method

3.1.2.1 Image Processing Procedure for Backlight Illumination Technology

The backlight illumination employed a background subtraction approach to isolate the spray features from the background, as shown in Figure 2. By subtracting the background image from the original image, a background difference image is obtained. Adjusting the binarization threshold allows for the creation of a binary image highlighting the spray. Subsequently, the boundaries of the liquid spray are extracted from this binary image, providing a clear representation of the liquid-phase spray in the backlight illumination images. The binarization threshold in this study is taken as 0.35.

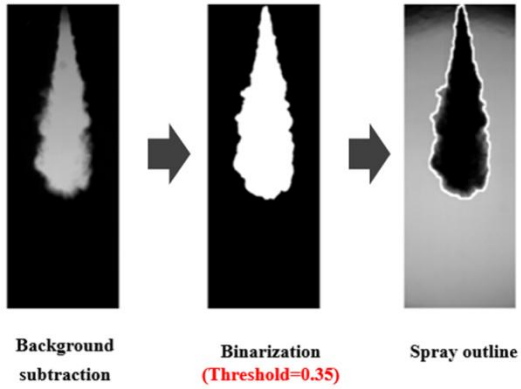

Figure 2. Backlight method image processing.

3.1.2.2 Image Processing Procedure for Schlieren Imaging Technology

The processing procedure of the Schlieren images is shown in Figure 3. The Schlieren image was processed with the frame difference method, which takes the pixel matrix difference between successive frames of the same spray image to enhance the visibility of dynamic spray features. Morphological operations were subsequently applied to refine the spray contours, and a sophisticated approach to multi-judgment was employed to eliminate isolated points that may arise as noise, ensuring the generation of a clear and comprehensive image representation of the vapor-phase spray.

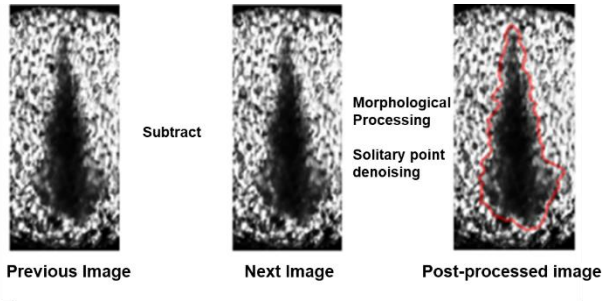

Figure 3. Schlieren method image processing.

3.1.3 Definition of Spray Characteristics

The definition of the spray characteristics is shown in Figure 4. The spray penetration length is defined as the maximum length along the nozzle axis from the tip of the nozzle to the farthest point of the fuel spray. The spray area is defined as the area of the identified spray region. Currently, there is no universally accepted definition for the spray cone angle. However, the general principle involves drawing two straight lines from the nozzle that encloses the outer boundary of the spray. The angle between these two lines is defined as the spray cone angle. In this study, the spray cone angle is defined as the vertex angle of an isosceles triangle, where the height and spray projection area of the triangle are equivalent to those of the spray region at 0.5 times the spray penetration length.

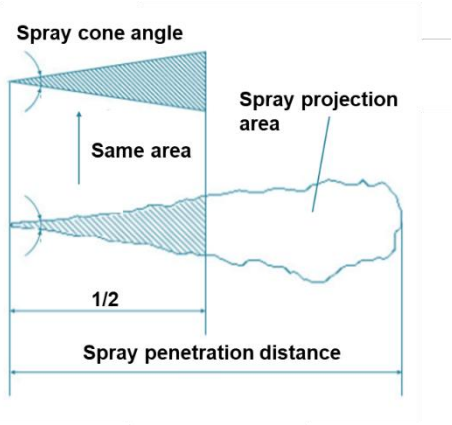

Figure 4. Definition of Spray characterization parameters.

3.1.4 Experimental Conditions of Spray Characteristics

The experimental conditions and the test fuels are summarized in Table 2, where the background pressure is fixed at 4 MPa, corresponding to a methanol saturation temperature of 473 K. When the background temperature is lower than the saturation temperature, it is considered a non-evaporative condition. The background temperatures of 800 K were tested in the present work, being evaporative conditions for methanol. In each experimental condition, the injection duration was set as 2.5 ms, and the measured spray characteristics were averaged over 5 repeated injections to obtain the final results for spray parameters.

Table 2. Experimental conditions for the spray characteristics.

Parameters	Values
Fuel	Methanol, Diesel, W10, W20, W30
Injection Pressure (MPa)	90
Background Temperature (K)	800
Background Pressure (MPa)	4

3.2 Introduction to Single-cylinder Engine and Experimental Conditions

3.2.1 Experimental Platform for Single-cylinder Engine

Table 3 lists the relevant parameters of the diesel-ignited high-pressure direct injection methanol combustion engine. Figure 4 provides a schematic

diagram of the single-cylinder engine. To enable diesel-ignited high-pressure direct injection methanol combustion, modifications were made to the structure of the cylinder head to accommodate a main injector for methanol fuel injection and a pilot injector for diesel ignition. The main injector is still located at the center of the original diesel engine, while the pilot injector is offset from the cylinder center and slightly inclined. The injection timing and duration of both high-pressure injectors can be controlled via an open electronic control unit (ECU). The injection pressure of the main injector can be flexibly adjusted within the range of 0-140 MPa, while the injection pressure of the pilot injector can be flexibly adjusted within the range of 0-180 MPa.

Table 3. Engine specifications.

Parameters	values
Bore/mm	129
Stroke/mm	155
Displacement/L	2
Compression ratio	16.5
Intake valve close/CAD ATDC	-159
Exhaust valve open/CAD ATDC	128
Methanol injector	10×0.2 mm×149°
Methanol injection pressure/MPa	0-140
Diesel injector	6×0.1 mm×140°
Diesel injection pressure /MPa	0-180

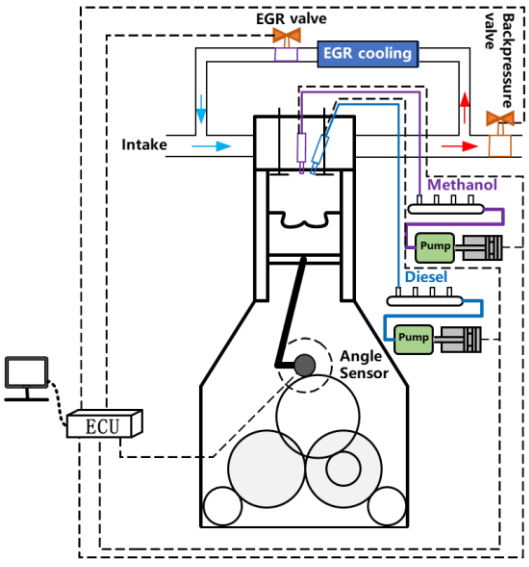

Figure 4. The schematic diagram of the single-cylinder engine.

The schematic diagram of the single-cylinder engine test system is shown in Figure 5. The engine operates at a constant speed maintained by an electric dynamometer. The intake air is simulated through a turbocharging system, with an intake control system regulating intake pressure and temperature. The fuel consumption of diesel and methanol is measured using Coriolis mass flow meters, with a flow range of 15 kg/h and an accuracy level of 0.1. In-cylinder pressure is measured by a Kistler 6125C pressure sensor and combustion characteristics such as heat release rate are calculated using the Kibox combustion analyzer. Gaseous emissions, including carbon monoxide (CO), unburned hydrocarbons (HC), and nitrogen oxides (NOx), are measured by a Gasboard-9801 exhaust gas analyzer. Exhaust smoke opacity is measured using an AVL439 opacity meter.

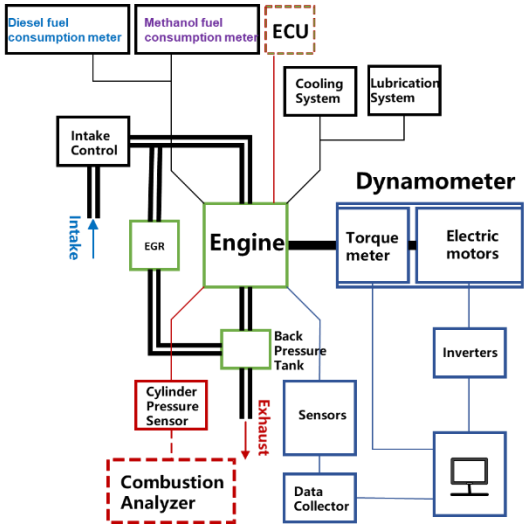

Figure 5. The schematic diagram of the single-cylinder engine experimental platform.

3.2.2 Experimental Conditions

Table 4. Experimental conditions.

Parameters	Values
Speed/rpm	1200
IMEP/bar	4/6/8/10/12
Intake pressure/bar	1.1/1.3/1.4/1.6/1.8
Diesel injection time/CAD BTDC	18/18/20/22/24
Diesel injection pressure /MPa	80
Methanol injection time /CAD BTDC	8/8/10/12/14
Methanol injection pressure /MPa	60
Methanol substitution rate/%	90-97

The experimental conditions are shown in Table 4. The tests were conducted at 1200 rpm, with a methanol injection pressure of 60 MPa and a baseline diesel injection pressure of 80 MPa. Diesel ignition of high-pressure direct injection methanol combustion was tested within a wide load range of 4-12 bar IMEP. A diesel-first, methanol-later injection strategy was adopted. The methanol substitution rate in the diesel ignition high-pressure direct injection methanol combustion was controlled within 90-97%. During the experiments,

the intake temperature was maintained at 32±3°C, while the coolant and lubricant oil temperature were both controlled at about 80°C.

4 RESULTS

4.1 Spray Characteristics under High Injection Pressure and Evaporative Conditions

4.1.1 Liquid-phase Spray Characteristics under High Injection Pressure and Evaporative Conditions

Figure 6 compares the liquid-phase spray development process of different fuels at a background temperature of 800 K. As shown in the figure, the liquid-phase sprays of all test fuels reach a quasi-steady state, exhibiting a slender, fluctuating spray tip. With increasing water content in methanol, both the length and width of the liquid-phase spray increase, and the fluctuation amplitude of the spray tip becomes more pronounced. This phenomenon can be attributed to the higher specific heat capacity and latent heat of vaporization of methanol-water blends. These properties allow the spray droplets to travel greater lengths before the complete evaporation. Consequently, the droplets at the spray tip experience the aerodynamic drag for a longer duration, thereby intensifying the instability of the spray tip.

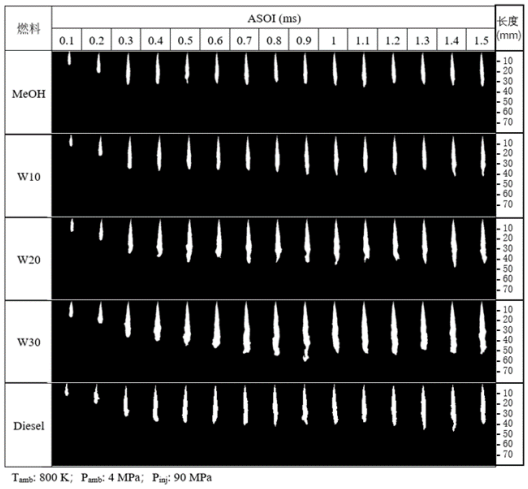

Figure 6. Comparison of the liquid-phase spray development process of methanol, W10, W20, W30, and diesel.

From Figure 7, it can be observed that at a background temperature of 800 K, the liquid-phase sprays of different test fuels all reach a quasi-steady state. The quasi-steady-state liquid-phase spray penetration lengths (L_{liquid}) for W10, W20, and W30 are 39.3 mm, 48.4 mm, and 54.8 mm, respectively, representing increases of 10%, 36%, and 54% compared to methanol (35.7 mm). This indicates that the quasi-steady-state liquid-phase spray penetration length significantly increases with the addition of water. This phenomenon can be attributed to the significant increase in the specific heat capacity and latent heat of vaporization of the fuel with higher water content. As a result, the heat required for droplet evaporation increases. Simultaneously, the viscosity and surface tension of the fuel also increase, which inhibits droplet breakup. Consequently, droplets must travel farther downstream to achieve complete evaporation, leading to an increase in the quasi-steady-state liquid-phase spray penetration length (L_{liquid}). Under these conditions, the quasi-steady-state liquid-phase spray penetration length (L_{liquid}) of W10 remains shorter than that of diesel, while those of W20 and W30 exceed that of diesel.

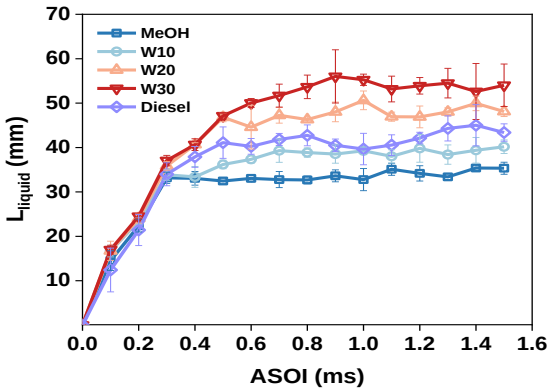

Figure 7. Comparison of the liquid-phase spray penetration length of methanol, W10, W20, W30, and diesel.

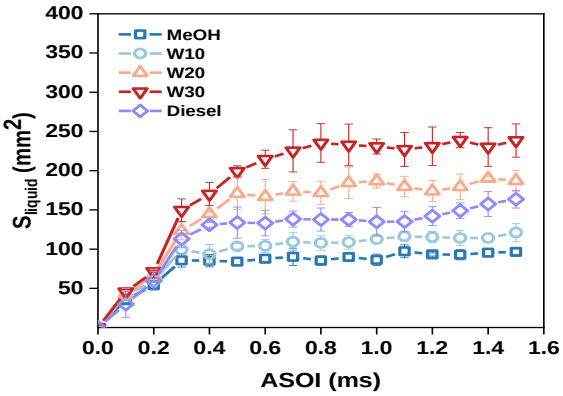

Figure 8. Comparison of the liquid-phase spray projection areas of methanol, W10, W20, W30, and diesel.

From Figure 8, it can be observed that at a background temperature of 800 K, the liquid-phase spray areas of different fuels all reach a quasi-steady state. The quasi-steady-state liquid-phase spray projection areas (S_{liquid}) for W10, W20, and W30 are 119 mm², 183 mm², and 240 mm²,

respectively, representing increases of 27%, 95%, and 158% compared to methanol (94 mm²). Notably, the quasi-steady-state liquid-phase spray projection areas (S_{liquid}) of W20 and W30 have already exceeded that of diesel.

From Figure 9, it can be found that there is little difference in the liquid-phase spray cone angles (θ_{liquid}) among the different test fuels. Although the droplet breakup and evaporation are weaker, resulting in a wider liquid-phase spray, the liquid-phase spray penetration length also increases. As a result, the liquid-phase spray cone angle (θ_{liquid}) shows minimal variation.

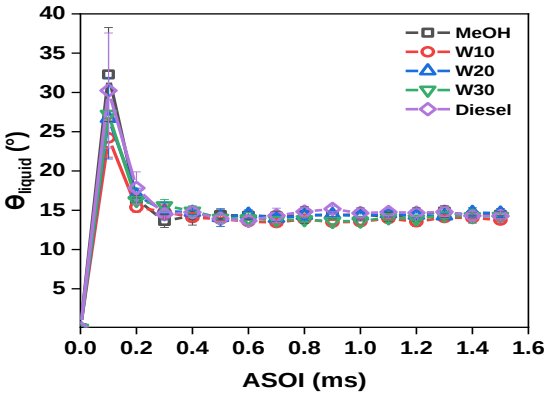

Figure 9. Comparison of the liquid spray cone angles of methanol, W10, W20, W30, and diesel.

4.1.2 Vapor-phase Spray Characteristics under High Injection Pressure and Evaporative Conditions

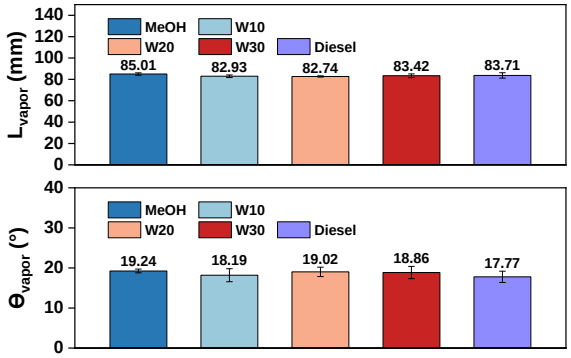

Figure 10. Comparison of the quasi-steady-state vapor-phase penetration length and spray cone angles of methanol, W10, W20, W30, and diesel.

Figure 10 compares the quasi-steady-state vapor-phase spray penetration lengths (L_{vapor}) and spray cone angles (θ_{vapor}) of methanol, W10, W20, W30, and diesel under conditions of a background temperature of 800 K, background pressure of 4 MPa, and injection pressure of 90 MPa. The vapor-phase spray penetration lengths (L_{vapor}) and spray cone angles (θ_{vapor}) of methanol, W10, W20, W30, and diesel exhibit minimal differences.

Figure 11 compares the quasi-steady-state vapor-phase spray projection areas (S_{vapor}) of methanol, W10, W20, W30, and diesel under conditions of a background temperature of 800 K, background pressure of 4 MPa, and injection pressure of 90 MPa. It can be observed that the vapor-phase spray projection areas of methanol, W10, W20, W30, and diesel show minimal differences. As the injection progresses, the liquid phase gradually transitions into the vapor phase, leading to a decreasing trend in the ratio of liquid-phase spray projection area to vapor-phase spray projection area (S_{liquid}/S_{vapor}). Additionally, higher water content inhibits the transition from the liquid phase to the vapor phase.

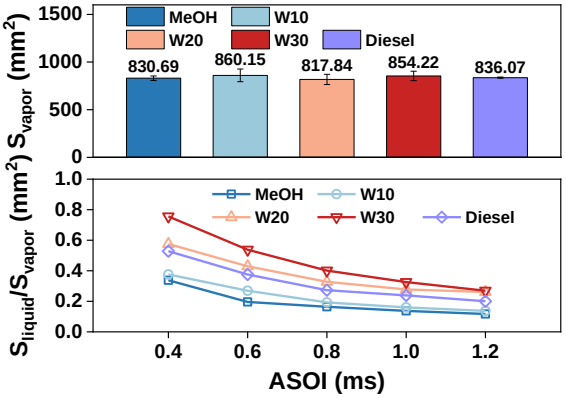

Figure 11. Comparison of the quasi-steady-state liquid-phase spray projection area methanol, W10, W20, W30, and diesel.

4.2 Experiments on Combustion and Emission Performance of Water-blended Methanol

4.2.1 Effects of Water Blending on Methanol Combustion Characteristics

The combustion performance of IMEP=4, 8, 12 bar (corresponding to low, medium, and high loads, respectively) is given in Figures 12 to 14. With the increase of water content, the high specific heat capacity of water leads to the absorption of heat in the combustion process, which reduces the combustion temperature, the in-cylinder pressure shows a downward trend, and the peak in-cylinder pressure decreases. Meanwhile, the instantaneous rise in in-cylinder pressure decreases due to the evaporation of water to absorb heat, which slows down the combustion rate.

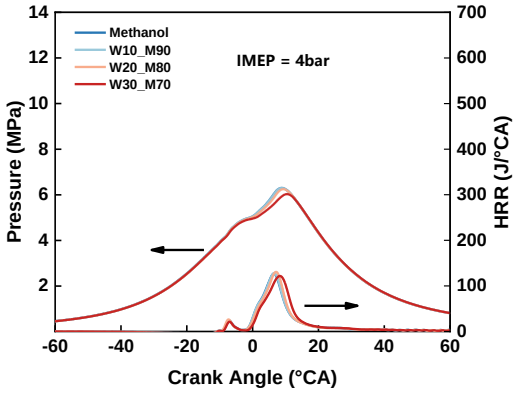

Figure 12. In-cylinder pressure and heat release rate at different operating conditions (IMEP = 4bar).

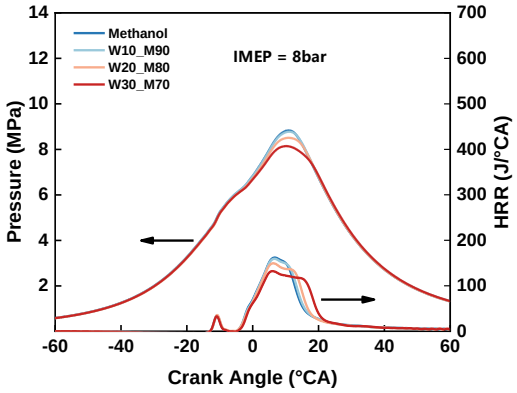

Figure 13. In-cylinder pressure and heat release rate at different operating conditions (IMEP = 8bar).

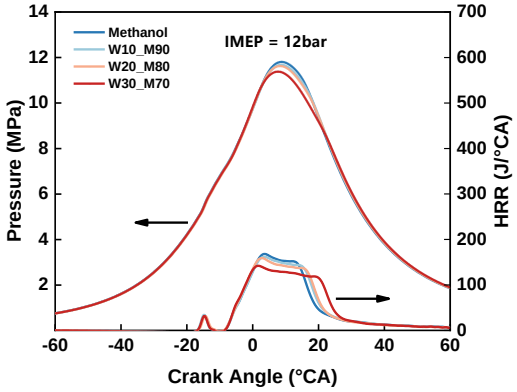

Figure 14. In-cylinder pressure and heat release rate at different operating conditions (IMEP = 12 bar).

At the same time, with the increase in water content, the peak value of the heat release rate curve decreases, and the curve becomes smoother. Specifically, under low water content (W10), the heat release rate exhibits a higher peak, indicating a more concentrated combustion process and faster heat release. The differences in cylinder pressure and heat release rate between W10 and methanol combustion are not significant.

At moderate water content (W20), the peak heat release rate is slightly lower than that of W10, but the combustion process is more stable. Under high water content (W30), the peak heat release rate is significantly reduced, the combustion process is delayed, and the overall heat release rate slows down.

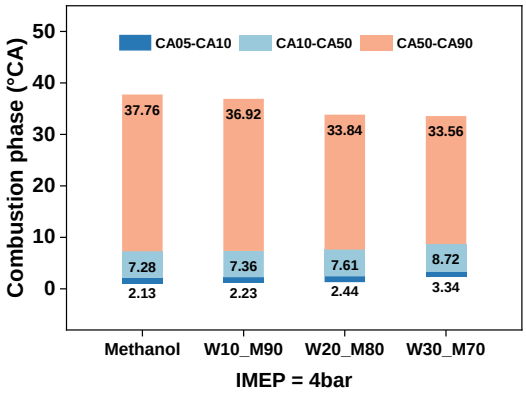

Figure 15. Combustion phase at different operating conditions (IMEP = 4 bar).

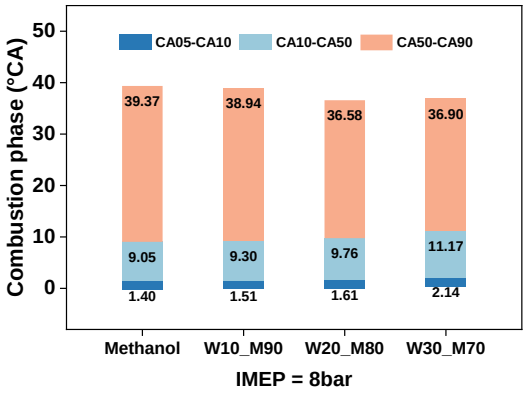

Figure 16. Combustion phase at different operating conditions (IMEP = 8 bar).

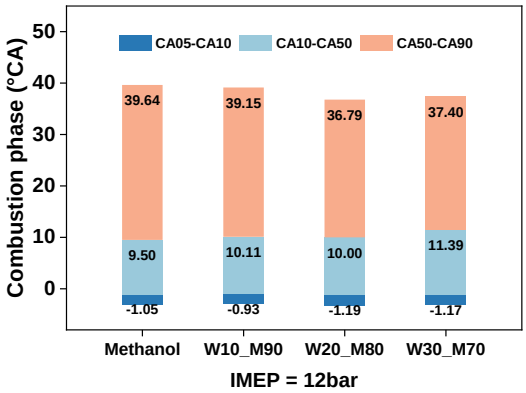

Figure 17. Combustion phase at different operating conditions (IMEP = 12 bar).

The combustion phase of IMEP=4, 8, 12 bar (corresponding to low, medium, and high loads,

respectively) is given in Figures 15 to 17. The numbers in the figures, from bottom to top, represent the crank angles corresponding to CA10, CA50, and CA90. At low and medium load conditions, with increasing water content, CA10 is delayed under different IMEP conditions, indicating a suppression of the premixed combustion phase and an extension of the premixed time. At the same time, CA50 is also delayed, reflecting a slower combustion rate and a delay in the heat release during the middle stage of combustion. Under high load conditions, due to the higher cylinder temperature and pressure at the end of the compression stroke, the thermal conditions within the cylinder during the early combustion stage are improved. As a result, the sensitivity of the variation of the early combustion phase to water content is reduced, and CA10 remains essentially constant. However, the increased water content extends the premixed phase, leading to a delayed CA50. This delay accelerates the combustion in the post-combustion stage (CA50-CA90), which shortens the overall combustion duration across different load conditions. This is beneficial for maintaining cylinder pressure during the post-combustion stage, thereby improving the effective power output.

4.2.2 Effects of Water Blending on Methanol Emission Characteristics

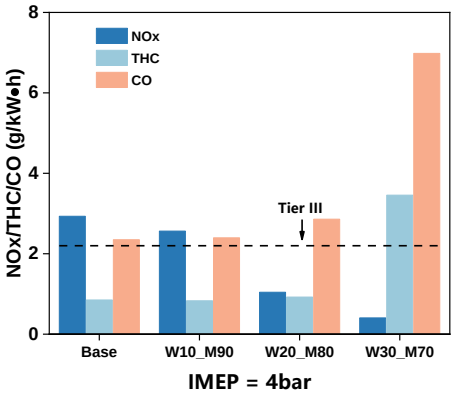

Figure 18. NOx、CO、HC emissions at different operating conditions (IMEP = 12 bar).

The major engine emissions of IMEP=4, 8, and 12 bar (corresponding to low, medium, and high loads, respectively) are given in Figures 18 to 20. At low load conditions, CO and HC emissions are highly sensitive to water content. As the water content increases, CO and HC emissions rise significantly, indicating a decline in combustion efficiency.

In contrast, under medium and high load conditions, due to the improved thermal conditions within the cylinder, although CO and HC emissions still show an overall increasing trend with higher water content, the differences are not significant, and the incomplete combustion losses remain relatively low. For NOx emissions, as the water content increases, the reduction in in-cylinder combustion temperature leads to a significant decrease in NOx emissions. Under low load conditions, a water content of 10% is sufficient to meet the Tier III emission standards, while under medium and high load conditions, higher water contents of 20% and 30% are required, respectively.

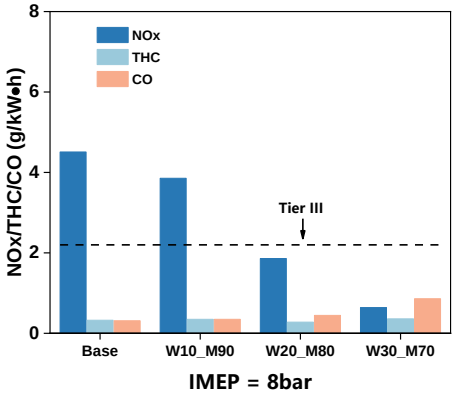

Figure 19. NOx、CO、HC emissions at different operating conditions (IMEP = 8 bar).

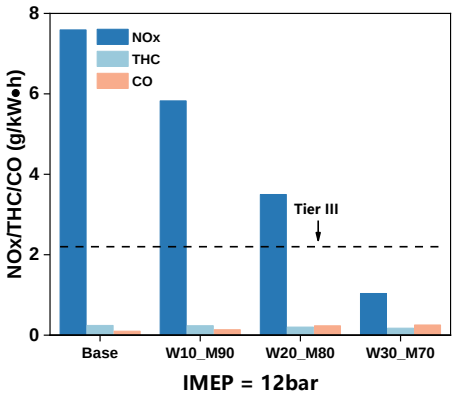

Figure 20. NOx、CO、HC emissions at different operating conditions (IMEP = 12 bar).

4.2.3 Effects of Water Blending on Methanol Energy Distribution

The energy distribution of IMEP=4, 8, 12 bar (corresponding to low, medium, and high loads, respectively) is given in Figures 21 to 23. With increasing water content, the total energy released from the fuel decreases due to the reduced calorific value of the combustion (as water does not contribute to combustion). Furthermore, the slower combustion rate causes a portion of the energy to be dispersed into incomplete combustion losses and other forms of losses, leading to a gradual decline in indicated thermal efficiency from

approximately 50% to 44%-47% under high water content conditions (W30).

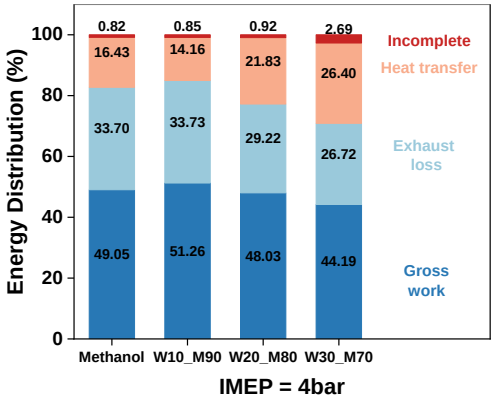

Figure 21. Energy distribution at different operating conditions (IMEP = 4 bar).

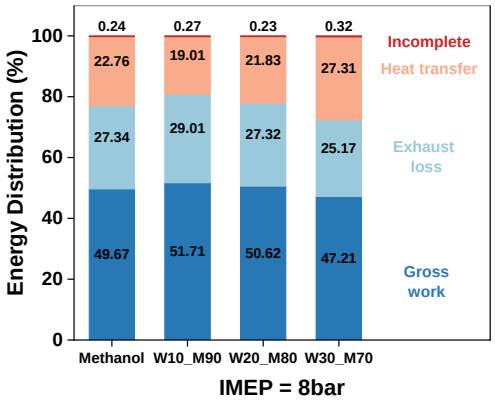

Figure 22. Energy distribution at different operating conditions (IMEP = 8 bar).

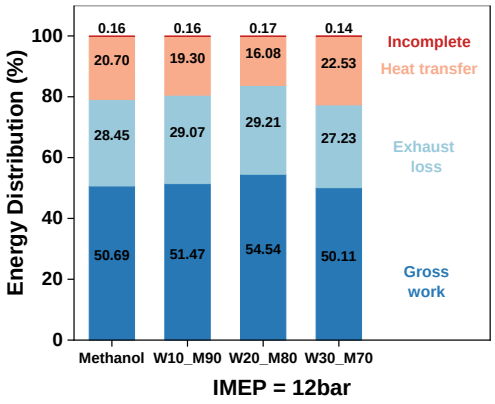

Figure 23. Energy distribution at different operating conditions (IMEP = 12 bar).

As water evaporates and absorbs heat, the in-cylinder combustion temperature decreases, which lowers the exhaust gas temperature, resulting in a gradual reduction in exhaust losses with increasing water content. Heat transfer losses, on the other hand, exhibit slight changes but generally show an upward trend as water content increases. At low water content, heat transfer losses account for a smaller proportion, but with higher water content (W30), heat transfer losses slightly increase. Under high water addition, a large amount of fuel is sprayed into the upper combustion chamber in the middle and late stages of injection, and the distribution of high-temperature area in the piston pit is reduced, so the heat transfer loss decreases. In front of the jet flame contact to the combustion chamber wall, due to higher near-wall tangential velocity, greater radial penetration distance of the jet flame, strengthening the flame-to-wall interaction, high-temperature areas more concentrated distribution near the cylinder wall, so the wall heat transfer increases. Incomplete combustion losses, as a whole, show an upward trend with increasing water content. Under low load conditions, the increase is more pronounced, while under high load conditions, the incomplete combustion losses remain relatively constant.

5 CONCLUSIONS

This study investigates the high-pressure spray characteristics of water-blended methanol and its combustion and emission performance in a single-cylinder dual direct injection engine. The main findings are summarized as follows:

1、 At a background temperature of 800 K, the quasi-steady liquid-phase spray penetration length and spray projection area increased significantly with water content. For water contents of 20% wt and 30% wt, the quasi-steady liquid-phase spray penetration length exceeded that of diesel. The vapor-phase spray penetration length, spray cone angle, and spray area of methanol, water-blended methanol, and diesel showed little difference. The effect of water addition on the liquid-phase spray characteristics of methanol was more significant, while its impact on the vapor-phase spray was minimal.

2、 Under low and medium load conditions, combustion rates and delayed heat release in the middle combustion phase were slowed with increased water content, resulting in delayed CA10 and CA50. At high load conditions, CA10 was less sensitive to water content. As water content increased, the intensity of the post-combustion (CA50-CA90) was enhanced, shortening the overall combustion duration.

3、 To meet Tier III emission standards, a water content of 10% was sufficient under low load conditions, while higher water contents of 20% and 30% were required for medium and high load conditions, respectively.

4、With the increase of water content, the indicated thermal efficiency gradually decreases from about 50% to 44%-47% at high water content conditions, the exhaust loss gradually decreases, the overall heat transfer loss increases slightly, and the incomplete combustion loss shows an increasing trend.

6 DEFINITIONS, ACRONYMS, ABBREVIATIONS

IMO	International Maritime Organization
EEDI	Energy Efficiency Design Index
IMEP	Indicate Mean Effective Pressure
BMEP	Brake Mean Effective Pressure
ASOI	After the start of the injection
W10	Methanol blended with 10% water
W20	Methanol blended with 20% water
W30	Methanol blended with 30% water
CO	carbon monoxide
UHC	unburned hydrocarbons
NOx	nitrogen oxides

7 ACKNOWLEDGMENTS

This work was supported by Excellent Young Scientists Fund Program (Overseas) (Admission No. 21FAA01116) and by the Science Fund for Creative Research Groups of the National Natural Science Foundation of China Project (No. 51921004).

8 REFERENCES AND BIBLIOGRAPHY

[1] The State Council of the People's Republic of China. (2021). China's Policies and Actions for Addressing Climate Change (White Paper). *Beijing: The State Council Information Office*.

[2] European Commission. (2023). Proposal for a Regulation of the European Parliament and of the Council on circularity requirements for vehicle design and on management of end-of-life vehicles, amending Regulations (EU) 2018/858 and 2019/1020 and repealing Directives 2000/53/EC and 2005/64/EC (COM/2023/451 final). *Brussels: European Commission.*

[3] United Nations Conference on Trade and Development (UNCTAD). (2024). Review of Maritime Transport 2024. *Geneva: United Nations*.

[4] International Maritime Organization (IMO). (2023). 2023 IMO Strategy on Reduction of GHG Emissions from Ships. *London: International Maritime Organization*.

[5] Sarathy SM, Oßwald P, Hansen N, Kohse-Höinghaus K. Alcohol combustion chemistry. Progress in Energy and Combustion Science 2014; 44: 40-102.

[6] Ampah, J.D., Yusuf, A.A., Afrane, S., Jin, C., Liu, H.F., 2021. Reviewing two decades of cleaner alternative marine fuels: towards IMO's decarbonization of the maritime transport sector. J*ournal of Cleaner Production*.

[7] International Maritime Organization (IMO). (2020). Interim Guidelines for the Safety of Ships Using Methyl/Ethyl Alcohol as Fuel (MSC.1/Circ.1621). London: International Maritime Organization.

[8] Felix S, Janos L.B., Remzi C.S., Thorsten S, Benedikt H, Ralf P, Detlef S. Methanol as a renewable energy carrier: An assessment of production and transportation costs for selected global locations, Advances in Applied Energy, 2021,100050.

[9] L.R. Clausen, N. Houbak, B. Elmegaard, Technoeconomic analysis of a methanol plant based on gasification of biomass and electrolysis of water, Energy. 2010.

[10] H. Li, H. Hong, H. Jin, R. Cai, Analysis of a feasible polygeneration system for power and methanol production taking natural gas and biomass as materials, Applied Energy. 87 (2010), https://doi.org/10.1016/j.apenergy.2009.07.001.

[11] S. Brynolf, M. Taljegard, M. Grahn, J. Hansson, Electrofuels for the transport sector: A review of production costs, Renew. Renewable and Sustainable Energy Reviews. 81 (2018).

[12] Ravikumar D, Keoleian G, Miller S. The environmental opportunity cost of using renewable energy for carbon capture and utilization for methanol production[J]. Applied Energy, 2020, 279.

[13] Verhelst S, Turner J W G, Sileghem L, et al. Methanol as a fuel for internal combustion engines[J]. Progress in Energy and Combustion Science, 2019, 70: 43-88.

[14] Yao C, Pan W, Yao A. Methanol fumigation in compression-ignition engines: A critical review of recent academic and technological developments[J]. Fuel, 2017, 209: 713-32.

[15] International Energy Agency - Advanced Motor Fuels (IEA-AMF). (2021). Methanol as motor fuel: Summary report. Paris: IEA-AMF.

[16] Hasan A O, Osman A I, Al-muhtaseb A A H, et al. An experimental study of engine characteristics and tailpipe emissions from modern DI diesel engine fuelled with methanol/diesel blends[J]. Fuel Processing Technology, 2021, 220.

[17] Sayin C, Ozsezen A N, Canakci M. The influence of operating parameters on the performance and emissions of a DI diesel engine using methanol-blended-diesel fuel[J]. Fuel, 2010, 89(7): 1407-14.

[18] Wang B, Yao A, Yao C, et al. In-depth comparison between pure diesel and diesel methanol dual fuel combustion mode[J]. Applied Energy, 2020, 278.

[19] Wang Q, Wei L, Pan W, et al. Investigation of operating range in a methanol fumigated diesel engine[J]. Fuel, 2015, 140: 164-70.

[20] Saccullo M, Benham T, Denbratt I. Dual Fuel Methanol and Diesel Direct Injection HD Single Cylinder Engine Tests[C]// SAE Paper. Detroit, Michigan, USA, 2018, 2018-01-0259.

[21] Jia Z, Denbratt I. Experimental investigation into the combustion characteristics of a methanol-Diesel heavy duty engine operated in RCCI mode. Fuel 2018;226:745-53.

[22] Dong Y, Kaario O, Hassan G, Ranta O, Larmi M, Johansson B. High-pressure direct injection of methanol and pilot diesel: A non-premixed dual-fuel engine concept. Fuel 2020;277.

[23] MAN Energy Solutions (2020). ME-LGIM engines operating at Methanol for large merchant marine vessels. MAN Energy Solutions.

[24] Lennart Haraldson, Wärtsilä R&D (2015). METHANOL AS FUEL.

[25] Aakko-Saksa PT, Westerholm M, Pettinen R, Soderstrom C, Roslund P, Piimakorpi P, Koponen P, Murtonen T, NiinistoM, Tuner M, Ellis J. Renewable Methanol with Ignition Improver Additive for Diesel Engines[J]. Energy & Fuels 2020, 34(1): 379-388.

[26] Ghosh, Anupam. (2020). Measurement of liquid penetration and vapour penetration of evaporating methanol sprays. Atomization and Sprays.

[27] Wang, Y.; Dong, P.; Long, W.; Tian, J.; Wei, F.; Wang, Q.; Cui, Z.; Li, B. Characteristics of Evaporating Spray for Direct Injection Methanol Engine: Comparison between Methanol and Diesel Spray. Processes 2022.

[28] Svensson, E., Li, C., Shamun, S., Johansson, B. et al., "Potential Levels of Soot, NOx, HC and CO for Methanol Combustion," SAE Technical Paper 2016-01-0887, 2016.

[29] MAN Energy Solutions (2018). MAN B&W two-stroke marine engines emission project guide for MARPOL Annex VI regulations. Augsburg, Germany: MAN Energy Solutions.

[30] MAN Energy Solutions. Four-stroke engine solutions for low-carbon and carbon-free fuels. MAN Energy Solutions.